# Mobility and dissociation of electronically excited Kr2+ ions in cold krypton plasma

Cyril van de Steen, Malika Benhenni, René Kalus, Rajko Ćosić, Florent X. Gadéa, Mohammed Yousfi

APS/123-QED

# Mobility and dissociation of electronically excited $Kr_2^+$ ions in cold krypton plasma.

Cyril Van de Steen,[1,2,*] Malika Benhenni,[2,†] René Kalus,[1,‡]
Rajko Ćosić,[1,3] Florent Xavier Gadéa,[4] and Mohammed Yousfi[2]

[1]*IT4Innovations, VSB - Technical University of Ostrava, 17. listopadu 2172/15, 708 00 Ostrava-Poruba, Czech Republic.*

[2]*Laboratoire Plasma et Conversion d'Energie, LAPLACE & UMR5213 du CNRS, Université de Toulouse III Paul Sabatier, 118 route de Narbonne, 31062 Toulouse Cedex, France.*

[3]*Department of Applied Mathematics, Faculty of Electrical Engineering and Computer Science, VSB - Technical University of Ostrava, 17. listopadu 2172/15, 708 00 Ostrava-Poruba, Czech Republic.*

[4]*Laboratoire de Chimie et de Physique Quantiques, IRSAMC & UMR5626 du CNRS, Université de Toulouse III Paul Sabatier, 31062 Toulouse Cedex 09, France.*

(Dated: July 29, 2019)

## Abstract

Collisions of electronically excited krypton dimers with krypton atoms are studied using a hybrid (quantum-classical) dynamical method, semi-empirical *diatomics-in-molecules* electronic Hamiltonian, and Monte Carlo modeling. Krypton dimer mobility in krypton gas and dimer disappearance rate constants have been calculated for a broad range of the reduced electric field and five lowest excited electronic states of the dimer ion. Comparison with calculations recently reported for the electronic ground-state krypton dimer ion and with available experimental data is also provided. Two groups of the electronic states of the krypton dimer ion, resulting from a spin-orbit induced splitting, have been analyzed separately. Importantly, for both groups of states, the theoretical results bracket the experimental ones, therefore, considering mixtures of electronically excited states may strongly improve the agreement between theory and experiment. In addition, the effect of rotational-vibrational excitations in electronically excited krypton dimer ions is assessed and shown to also lead to an improved agreement between theory and experiment.


PACS numbers: 34.50.-s 52.20.-j 52.20.Hv 52.25.Fi


*Electronic address: cyril.vds@gmail.com

†Electronic address: malika.benhenni@laplace.univ-tlse.fr

‡Electronic address: rene.kalus@vsb.cz

## I. INTRODUCTION

Molecular ions play an important role in the development of low-temperature plasmas, generated more particularly at atmospheric pressure, in heavy rare gases [1, 2]. These low-temperature (or cold hereafter) plasmas can be used in various applications as, for instance, in plasma medicine and/or spacecraft propulsion [3, 4]. In plasma discharges dedicated to plasma medicine, He and Ar are mainly used as carrier gases but more recently, krypton is gaining interest in different plasma discharge experiment in admixture with He and Ar rather than alone because of its high cost. Indeed, Li et al [5] reported in their experiment that plasma jet using krypton as carrier gas exhibits different behavior than those using He or Ar, so it is interesting to further investigate krypton to get more insight. A large difference was observed in optical spectra for krypton in plasma jet experiment. And this may favor the production of different active species necessary for specific application in biomedicine. In order to better control and tailor the space-charge electric field magnitude and, therefore, the formation of many active species (radicals, excited species, charged particles, photons, etc.) in these weakly ionized rare gases, the basic data of the ion transport and reactivity are particularly needed in fluid models giving the spatial-temporal description and optimization of the cold plasma characteristics, like densities and temperatures of the main active species.

The fact that molecular ions play a role in cold plasmas is not surprising for rare-gas (Rg) dimer ions ($Rg_2^+$) since, in contrast to their neutral counterparts ($Rg_2$), they are quite strongly bound (see Table I) and easily survive under ambient conditions. Even the binding energy of ionic rare-gas trimers ($Rg_3^+$) is large enough for them to be non-negligibly populated at ambient temperature. For example, the binding energy of the krypton trimer ion is about 0.23 eV with respect to the $Kr_3^+ \rightarrow Kr_2^+ + Kr$ dissociation channel [6].

Two dominant mechanisms have been proposed for the formation of ionic rare-gas dimers in cold rare-gas plasmas [1], a *three-body recombination process*,

$$Rg^+ + Rg + Rg \rightarrow Rg_2^+ + Rg \tag{1}$$

and an *associative ionization (Hornbeck-Molnar) process* [7],

$$Rg^* + Rg \rightarrow Rg_2^+ + e^-. \tag{2}$$

In principle, electronically ground-state as well as excited dimers may be formed in both processes. For example, in the three-body recombination reaction, Eq. (1), ionic monomers

in their fine-structure ground-state, $^2P_{3/2}$, may be involved as well as excited ones, $^2P_{1/2}$. Both monomer species have been detected experimentally (for krypton see, e.g., Ref. 8).

The lowest electronic states of the $Kr_2^+$ ion are shown in Fig. 1 (and in Table I). As is clear from the figure, the ground-state ($^2P_{3/2}$) ionic monomer leads, in the collision with a neutral atom, to a diatomic complex in one of the group I states. These states comprise either the dimer ground state, $I(1/2)_u$, or excited states $I(3/2)_g$, $I(3/2)_u$ and $I(1/2)_g$. Electronically excited monomers ($^2P_{1/2}$), on the other hand, form ionic dimers in the group II states, either $II(1/2)_u$ or $II(1/2)_g$. Since it is known that the dynamics of rare-gas molecular ions is quasiadiabatic within each group of states [9], the recombination process of Eq. (1) is expected to lead to $Rg_2^+$ ions in one of the group I states if a $^2P_{3/2}$ ionic monomer is involved and to a group II state for the $^2P_{1/2}$ atomic ion. This quasiadiabaticity is due to a gap between group I and group II states resulting from the spin-orbit (SO) interaction and is thus the more pronounced, the stronger the SO interaction is. As a consequence, even electronically highly excited ionic dimers (states II) may be formed under ambient conditions. Moreover, they may survive for quite a long time due to their metastability [10, 11]. Excited electronic states may thus play an important role in cold rare-gas plasmas, particularly if heavier rare gases like krypton are involved. Therefore they deserve adequate attention, which is not particularly seen in up to now published literature.

The present work aims at partly filling this gap. It represents a continuation of our previous calculations on electronically ground-state $Kr_2^+$ ions [12] and extends them to the realm of electronically excited species. The main question we ask and try to answer here is whether the assumption of the presence of electronically excited $Kr_2^+$ ions in cold krypton plasma is consistent with available experimental data [1]. The paper is organized as follows. Firstly, a short survey of the methods we have used in the present calculations is provided in Sec. II. Then, selected results are presented in Sec. III, more specifically, the $Kr_2^+$ mobility in krypton gas is discussed in Subsec. III A and the dimer disappearance rate is reported and analyzed in Subsecs. III B and III C (with a complete summary of calculated data provided in a supplementary information material [13]). Finally, conclusive remarks and outlooks are provided in Sec. IV.

## II. METHODS AND COMPUTATIONS

The methodology used in the present work is basically the same as that used in our previous calculations on krypton ions [12, 14]. Consequently, only a brief summary is provided here and the reader is referred to the cited papers for further details.

### A. Interactions and dynamics

Shortly, the *diatomics-in-molecules* (DIM) [15] approach as applied to rare-gas cluster cations [16, 17] has been used to model the interactions in the $Kr_2^+/Kr$ collision complex, together with a simple scheme for the inclusion of the spin-orbit (SO) coupling [17, 18]. A couple of independent inputs are required for this, namely, the diatomic potentials for the ionic dimer fragment ($Kr_2^+$) with the SO interaction neglected (electronic ground-state, $^2\Sigma_u^+$, and three lowest excited states, $^2\Pi_g^+$, $^2\Pi_u^+$, $^2\Sigma_g^+$), the ground-state potential ($^1\Sigma_g^+$) for the neutral dimer fragment ($Kr_2$), and the SO coupling constant for the atomic ion ($Kr^+$).

Like in preceding studies [12, 14], two sets of ionic diatomic potentials have been used; one of a purely *ab initio* nature [19] (model A) and another combining *ab initio* calculations with accurate spectroscopic measurements [20] (model B). While model B seems more accurate for the electronic ground state of the $Kr_2^+$ ion [12, 14], model A is expected to perform somewhat better for the highly excited states of group II [21]. For the neutral dimer potential, a semi-empirical curve [22] has been used and, finally, the SO coupling constant has been taken from measurements [23].

The cross-sections needed for calculations of dimer ion transport properties and dissociation rates have been obtained from a quasiclassical trajectory approach. Hybrid (quantum-classical) equations of motion based on the Ehrenfest mean-field approach [24],

$$\dot{x}_\alpha = \frac{p_\alpha}{m_\alpha}, \quad \dot{p_\alpha} = \langle\psi| - \frac{\partial \hat{\mathrm{H}}}{\partial x_\alpha}|\psi\rangle, \tag{3}$$

$$i\hbar\frac{\partial\psi}{\partial t} = \hat{\mathrm{H}}\psi, \tag{4}$$

have been used to model the dynamical evolution of bunches of trajectories. Atomic nuclei, with positions $x_\alpha$ and momenta $p_\alpha$ ($\alpha = 1, \ldots, 9$ for the $Kr_2^+/Kr$ collision complex), have been treated classically [25] and propagated in time on a manifold of electronic states provided by the DIM model. The electronic subsystem has been treated quantum mechanically

and represented by its current electronic wave function ($\psi$) and corresponding DIM Hamiltonian ($\hat{\mathrm{H}}$). A particular implementation of the hybrid method used in the present work was described in detail in Ref. [26].

In addition to the coherent evolution represented by Eqs. (3) and (4), quantum decoherence has also been taken into account by periodically quenching the current electronic wave function to one of available adiabatic states and subsequently rescaling nuclear velocities (so that the total energy of the system is conserved). See Ref. 27 for necessary details. Particular implementation of the inclusion of quantum decoherence in the present calculation has been taken from our preceding work [12].

Bunches of trajectories have been evolved from initial conditions prepared in the same way as in the preceding study (see Subsec. 2.2.3 of Ref. 12 for a detailed description). The only difference consists in the fact that electronically excited potential energy curves have been used to describe the initial state of the dimer ion in the present work instead of the ground-state curve which was used in Ref. 12. Note also that both dimer ions prepared initially in their rotational-vibrational ground state and rotationally-vibrationally excited dimers have been considered (see Subsec. III A 2). The procedure of sampling inter-atomic distances and atomic velocities in rotationally-vibrationally excited dimers was described in detail in the preceding publication [12] and has been adopted here without any modification.

For each choice of the initial electronic state of the $Kr_2^+$ ion, for each initial rotational-vibrational state, and for each collision energy, bunches of tens to hundreds of individual trajectories have been used to calculate cross-sections. These bunches consist of subsets of about 500 trajectories corresponding to particular values of the collision impact-parameter sampled between $b = 0$ and $b = b_{\max}$ with a step of $\Delta b = 0.1\,\text{Å}$ and with $b_{\max}$ chosen such that convergence is achieved for both momentum-transfer and dissociative cross-sections.

### B. Collision cross-sections

Two kinds of processes result from collisions of $Kr_2^+$ ions with carrier gas atoms (Kr), the *non-reactive scattering* (NRS),

$$Kr_2^+ + Kr \rightarrow Kr_2^+ + Kr, \tag{5}$$

and the *dimer ion disappearance* (DID) scattering. The latter channel is usually identified with the *collision induced dissociation* (CID),

$$\mathrm{Kr}_2^+ + \mathrm{Kr} \rightarrow \mathrm{Kr}^+ + \mathrm{Kr} + \mathrm{Kr}, \tag{6}$$

but, as discussed below in Subsec. III C, a *charge transfer* (CT) channel, as well resulting in the ionic dimer disappearance, but accompanied by the formation of a stabilized neutral dimer instead of the emission of departing monomers,

$$\mathrm{Kr}_2^+ + \mathrm{Kr} \rightarrow \mathrm{Kr}^+ + \mathrm{Kr}_2, \tag{7}$$

should also be considered if electronically excited states of the colliding dimer ion are involved.

Like in the preceding works, momentum-transfer (MT) cross-sections are applied to the NRS channel,

$$\sigma_{\mathrm{NRS}}^{(\mathrm{MT1})} = \int_{4\pi} \left[\frac{\mathrm{d}\sigma}{\mathrm{d}\Omega}\right]_{\mathrm{NRS}} (1 - \cos\theta)\, \mathrm{d}\Omega, \tag{8}$$

$$\sigma_{\mathrm{NRS}}^{(\mathrm{MT2})} = \int_{4\pi} \left[\frac{\mathrm{d}\sigma}{\mathrm{d}\Omega}\right]_{\mathrm{NRS}} \left(1 - \frac{p'}{p}\cos\theta\right) \mathrm{d}\Omega, \tag{9}$$

and the total effective cross-section,

$$\sigma_{\mathrm{DID}}^{(\mathrm{int})} = \int_{4\pi} \left[\frac{\mathrm{d}\sigma}{\mathrm{d}\Omega}\right]_{\mathrm{DID}} \mathrm{d}\Omega, \tag{10}$$

are used for the CID and CT (DID) channels. The reason for using the MT cross-sections for the NRS processes is that the total effective cross-section diverges within the classical description if elastic scattering is included, while this divergence is removed if the MT approximation is adopted. The use of MT cross section is considered as an approximation to indirectly take into account the collision anisotropy without using differential cross section. This approximation proved to be a good one since a deviation of about 2% was found between the two approaches in the cases of $\mathrm{He}^+$ and $\mathrm{Ar}^+$ collisions with their parent gas [28, 29]. Note also that two kinds of the MT cross-section have been used, the standard one (Eq. (8)) proposed originally for the elastic scattering [30] and another (Eq. (9)) we used previously [31] to approximately include non-elastic effects in the dimer-monomer collisions.

### C. Monte Carlo simulations

Various transport properties can be obtained from pre-calculated cross-sections via Monte Carlo (MC) simulations [32]. To save space and preserve clarity of the present work, only

the $Kr_2^+$ mobility in krypton gas and its stability against collisions with gas atoms will be considered here (see Sec. III).

The MC method [32] is based on a series of one-by-one performed calculations of a sufficiently large number of stochastic trajectories representing the $Kr_2^+$ ion moving under the influence of a uniform external electric field (applied along the $z$ axis). Here, weakly ionized gas is considered and, thus, only ion-neutral ($Kr_2^+$/Kr) collisions are allowed. Standard reduced mobility ($K_0N$) and DID rate constant ($k_{\mathrm{DID}}$) are calculated for given ambient conditions from the mean DID frequency ($\langle\nu_{\mathrm{DID}}\rangle$) and velocity components ($v_z$) with:

$$K_0N = \frac{\langle v_z\rangle}{(E/N)}\frac{T_0}{T}\frac{P}{P_0} \tag{11}$$

and

$$k_{\mathrm{DID}} = \frac{\langle\nu_{\mathrm{DID}}\rangle}{N}, \tag{12}$$

where $P$ and $T$ are the pressure and temperature of the carrier gas, respectively, $T_0 = 273.16\,\mathrm{K}$, $P_0 = 760\,\mathrm{torr}$, and $N$ is the particle density of the carrier gas.

## III. RESULTS AND DISCUSSIONS

As mentioned in the preceding section, only selected results will be reported here, namely, $Kr_2^+$ mobilities and the dimer ion disappearance (DID) rate constants. The ion mobility is included since accurate experimental values are available in the literature [1] (as well as their extension via an inverse-method approach [33]) and a comparison with them allows to analyze the validity of the assumption that electronically excited $Kr_2^+$ dimers are present in weakly ionized krypton gas. The DID rate is then included to assess the stability of electronically excited $Kr_2^+$ ions in collisions with Kr atoms.

### A. Mobilities

There are plenty of experimental reports on the mobility of the $Kr_2^+$ ion in krypton, see Ref. 12 for a comprehensive summary. Among them, the measurements by Helm and Elford [1] seem to be the most reliable ones. For clarity, only these data will be considered here together with an inverse-method extension [12] allowing a comparison at reduced electric fields not covered by the measurement. The discussion will be provided separately for the

$Kr_2^+$ ions initially populating electronic states of group I and those of group II. As mentioned in Sec. I, the two populations of states can be presumed more or less independent of each other since a quasi-adiabaticity is expected [9] for the dynamics running on each manifold.

### *1. Group I electronic states*

Reduced mobilities of the $Kr_2^+$ ion excited, prior to its collision with a Kr atom, to one of the electronic states belonging to group I are summarized in Fig. 2. For simplicity, only rotationally-vibrationally ground states on respective potential energy curves are considered. Note that the data calculated previously for the ground-state dimer [12] are also included for comparison. Both interaction models introduced in Subsec. II A, model A [19] and model B [20, 34], and data calculated using both $\sigma_{\rm NRS}^{\rm (MT1)}$ and $\sigma_{\rm NRS}^{\rm (MT2)}$ momentum-transfer (MT) cross-sections (Eqs. (8) and (9), respectively) are considered.

The most important observations which are clear from Fig. 2 basically follow those made previously for the ground-state dimer [12]. Firstly, the $\sigma_{\rm NRS}^{\rm (MT1)}$ and $\sigma_{\rm NRS}^{\rm (MT2)}$ mobility data are close to each other and the effects of inelastic transfer of collision energy to the rotational and/or vibrational degrees of freedom of the dimer ion does not seem much important even if electronically excited states are involved.

Secondly, the data calculated for model A differ visibly from corresponding data obtained via model B. Except for high collision energies, the $Kr_2^+$ mobilities calculated using model B lie mostly above those obtained from model A. As mentioned above, while model B may be considered more accurate for the $Kr_2^+$ electronic ground state [12], the situation is not as clear for excited states. For example, the binding energies calculated for electronically excited states of $Kr_2^+$ using model B are always below respective values obtained from model A (see Table I). The semi-empirical potentials of model B may thus not be as accurate for higher electronic states as for the ground state.

Thirdly, the $Kr_2^+$ mobility decreases as the electronic state of the ion increases. Since all the data obtained for the electronically excited dimer lie below the experiment and since rotational-vibrational excitations are expected to further decrease the dimer mobility [12], it is not likely that excited states of group I dominate in experimental populations. On the other hand, however, if mixed populations of ground-state dimers and electronically excited dimers are assumed, a good agreement with the experiment can be achieved. This

is illustrated in the inset of Fig. 2 where a mixture of 70 % of ground-state dimers and 30 % of dimers occupying the most strongly bound excited state, $I(3/2)_g$, is considered. The presence of electronically excited dimers is thus not excluded in the experiment.

*2. Group II electronic states*

Mobility data calculated under the same conditions as for group I are shown in Fig. 3. As expected, the data obtained for model A and model B differ noticeably from each other. Since, as discussed above, model A may be more reliable than model B for $Kr_2^+$ excited states, we will adhere to it throughout the discussion. Further, while for the $II(1/2)_g$ state the data obtained from $\sigma_{NRS}^{(MT1)}$ and $\sigma_{NRS}^{(MT2)}$ cross-sections are close to each other, they differ visibly (by about $5-10$ %) for the $II(1/2)_u$ state, in particular, if weak electric fields are considered. The $\sigma_{NRS}^{(MT2)}$ cross-sections are however preferred since they may be more appropriate for expectedly inelastic collisions [35].

In general, the mobility values calculated for the dimer ion prepared initially in the $II(1/2)_u$ state overestimate the experimental data and the reverse holds for $II(1/2)_g$. In principle, it is thus possible to reproduce the experiment by properly mixing the data of these two data sets, as done in Fig. 3 (small circles). An overall agreement with the experimental data is achieved by mixing the $II(1/2)_u$ and $II(1/2)_g$ data with roughly the same weights. However, since it is unlikely that the weakly bound $II(1/2)_g$ state could survive at such a high abundance, mixing of the two group II states does not seem to properly account for the $Kr_2^+$ mobility observed experimentally.

Another way to get closer to the experimental points is to decrease the $II(1/2)_u$ estimates by considering the $Kr_2^+(II(1/2)_u)$ dimer populating, prior to its collision with a Kr atom, excited rotational-vibrational states. How such initial rotational-vibrational excitations influence calculated $Kr_2^+$ mobilities is demonstrated in Fig. 4. As expected [12], the mobility of the $Kr_2^+$ ion is reduced if the ion enters the collision either rotationally or vibrationally excited. Moreover, quite high initial excitations are required to get close to the experiment. This may indicate that rotationally-vibrationally excited $Kr_2^+$ dimers of group II are quite abundant in experimental populations. See also Subsecs. 3.2.2 and 3.3.2 of Ref. 12 where a similar observation is reported for the electronic ground state, $I(1/2)_u$.

In Fig. 4, the initial rotational and vibrational states of the dimer ion are selected so that

corresponding excitation energies are roughly the same. This allows to assess the efficiency of the two kinds of excitations in influencing the mobility of electronically excited $Kr_2^+$ ions. Unlike the electronic ground state where both excitations are more or less equally efficient [12], rotational excitations reduce the mobility of electronically excited ions much less than vibrational excitations, which particularly holds in the weak-field region. For example, approximately the same excitation energy corresponds to $[j = 130, v = 0]$ and $[j = 0, v = 10]$, but the $[j = 130, v = 0]$ excitation leads, in the weak-field region, to a decrease of the $Kr_2^+$ mobility which is only one half (or less) of that obtained for the $[j = 0, v = 10]$ case. Only in the limit of strong fields ($E/N \geq 400\,\mathrm{Td}$), do the two kinds of excitation become equally efficient. Different shapes of the rotation-free potential energy curve involved for $[j = 0, v = 10]$ and the effective potential containing centrifugal term in the case of $[j = 130, v = 0]$ must be beyond this observation. Since, the $\mathrm{II}(1/2)_\mathrm{u}$ state is much less strongly bound than the electronic ground state, this shape effect is more pronounced for the former.

### B. Dimer ion disappearance rates

Electronically excited $Kr_2^+$ ions are much less strongly bound than the ground-state dimer and dissociate (Eq. (6)) thus more easily after colliding with Kr atoms. Moreover, the charge transfer channel (Eq. (7)), which also leads to the disappearance of the ionic dimer, may as well be effective for some excited states. As a consequence, the dimer ion disappearance (DID) deserves attention. A survey of DID rates is provided in Figs. 5 and 6.

In Fig. 5, DID rate constants are displayed for all the electronic states of the colliding dimer and corresponding rotational-vibrational ground states. In addition, DID cross-sections are also displayed in the inset. If the DID cross-sections are inspected first, one can see that their behavior is mainly influenced by the binding energy of the ion in a particular electronic state (see Table I). In general, the magnitudes of the DID cross-sections grow up as the binding energy decreases and, expectedly, their thresholds move to lower collision energies. The DID rate constants basically follow the trends seen for cross-sections. Moreover, it is clear from the main panel of Fig. 5 that the model A and model B data differ significantly from each other for some states, $\mathrm{II}(1/2)_\mathrm{g}$, $\mathrm{I}(3/2)_\mathrm{u}$, and $\mathrm{I}(1/2)_\mathrm{g}$. This highly probably reflects the quite big differences in the binding energies calculated for these states

from the two models (see Table I).

The dependence of DID rates on the initial rotational-vibrational state of the colliding dimer ion is investigated for the $II(1/2)_u$ electronic state in Fig. 6. Like for mobilities, only data calculated using model A are shown in the figure for clarity. Clearly, initial rotational-vibrational excitations have a qualitatively similar effect on the calculated rate constants as electronic excitations - the higher is the state, the higher is the ion disappearance probability. In addition, rotational excitations seem to be less efficient in this respect than vibrational excitations.

### C. Production of stabilized neutral dimers

An interesting feature seen in the inset of Fig. 5 is that the DID cross-sections obtained for the $I(1/2)_g$ and $II(1/2)_g$ states have their thresholds, if any, well below corresponding binding energies ($D_0 = 0.013\,\mathrm{eV}$ and $D_0 = 0.026\,\mathrm{eV}$, respectively). This may mean that, for these two states, some extra energy is released during the DID. For example, the charge transfer (CT) channel (Eq. (7)) may contribute and lead to stabilized neutral dimers. As a result, the binding energy of the dimer is released and may decrease the DID threshold.

Such an assumption is, however, in contradiction with a usual view that, upon a charge hop, the neutral dimer explodes rapidly because its equilibrium geometry is heavily different from the geometry of the $Kr_2^+$ ion. But, while this basically holds (see Fig. 1 and Table I) for the electronic ground state of the ionic dimer, $I(1/2)_u$, and also for some excited states, $I(3/2)_g$ and $II(1/2)_u$, for the other states, namely, $I(1/2)_g$, $I(3/2)_u$ and $II(1/2)_g$, the situation is quite different. For these states, the equilibrium geometries of $Kr_2^+$ and $Kr_2$ are rather close to each other and the CT does not lead to a neutral dimer far from its equilibrium configuration. Since, further, the potentials of the three $Kr_2^+$ excited states are very shallow, possible rotational-vibrational excitations are small and stabilized $Kr_2$ may be produced.

The efficiency of the CT channel is demonstrated for the $II(1/2)_g$ state in Fig. 7 where the total cross-section of the overall DID channel is decomposed into contributions due to CID (Eq. (6)) and CT (Eq. (7)) processes. Clearly, both channels contribute comparably, though their efficiency may depend on the collision energy. Surprisingly, the production of neutral dimers through the CT channel is non-negligible even at high collision energies.

In the inset of Fig. 7, distributions of the appearance probability of the neutral dimer are

displayed for selected collision energies over contributing impact-parameters. The almost flat distribution seen for the lowest collision energy considered in Fig. 7 ($E_{\mathrm{coll}} = 0.08\,\mathrm{eV}$) probably indicates that statistical behavior dominates over dynamics at low kinetic energies. Noteworthy, mostly long-lived (orbiting) trajectories have been observed in our calculations in the low-energy region and quite long times have been needed for the $Kr_2^+/Kr$ collision complex to disintegrate. For higher collision energies, on the other hand, dynamics becomes important, as documented by more complex distributions obtained in this case. Quite understandably, no charge transfer is observed for impact-parameters above $b \approx 7\,\text{Å}$. The close to zero probability of the CT channel seen at small impact-parameter values ($b \leq 2 - 3\,\text{Å}$) may, on the other hand, originate from increased importance of the CID for these, almost head-on collisions.

## IV. CONCLUSIONS

Collisions of electronically excited ionic dimers of krypton, $Kr_2^+$, with krypton gas atoms have been studied using a hybrid dynamical approach [26, 27] (classical treatment of heavy nuclei and quantum description of light electrons) and a semi-empirical electronic Hamiltonian based on the *diatomics-in-molecules* approximation [16, 17]. Data we previously obtained for the ground-state ionic dimer [12] have also been considered for comparison. The effect of the electronic excitation in the $Kr_2^+$ ion on its mobility in krypton gas and on the $Kr_2^+$ stability against collisions with krypton atoms have been analyzed for a broad range of the reduced electric field ($E/N = 5 - 3000\,\mathrm{Td}$). Only selected data are reported in the paper, a complete set of calculated results is provided in a supplementary information material [13].

The theoretical data on the $Kr_2^+/Kr$ mobility have been compared with experimental values [1] and it has been found that the assumption of the presence of electronically excited dimer ions in cold krypton plasma is compatible with the experiment. In general, an excellent agreement with the experiment is achieved if properly adjusted abundances of various electronic and/or rotational-vibrational excitations are considered. However, no quantitative conclusions about these abundances can be derived since there are too many uncontrolled parameters. As a consequence, additional calculations, particularly calculations on the mechanisms of the formation of the $Kr_2^+$ ions and on the relaxation of their

nascent (electronic) excitations, are needed to shed more light on this issue.

Calculated diatomic ion disappearance rates have shown that there is a qualitative correspondence between them and the strength of the $Kr_2^+$ bond in particular electronic states. Among others, this confirms our former observation [9] that the dynamics of rare-gas cluster cations is more or less quasiadiabatic within manifolds of electronic states asymptotically correlating to either $^2P_{3/2}$ or $^2P_{1/2}$ fine-structure states of the atomic ion ($Kr^+$).

Another interesting finding following from the present calculations is that, for some electronic states of the $Kr_2^+$ ion, $II(1/2)_g$, in particular, but to some extent also for $I(3/2)_u$ and $I(1/2)_g$, stabilized neutral dimers are formed at a non-negligible amount. This observation is interpreted in terms of charge transfer between the ionic dimer and the impacting neutral atom, $Kr_2^+ + Kr \rightarrow Kr^+ + Kr_2$, which may lead to a stabilized neutral dimer if equilibrium geometries of the ionic parent and the neutral daughter are close to each other and the rotational-vibrational excitation of the ionic parent dimer is not high. As discussed in Subsec. III C, these conditions are satisfied, e.g., for the $II(1/2)_g$ state of the $Kr_2^+$ ion, for which, really, a non-negligible rate of production of stabilized neutral dimers has been recorded.

In summary, the present work clearly shows that electronically excited $Kr_2^+$ ions may play a role in cold krypton plasma. Moreover, the populations of dimers occupying electronic states of group I – $I(1/2)_u$, $I(3/2)_g$, $I(3/2)_u$ and $I(1/2)_g$, and those in states of group II – $II(1/2)_u$ and $II(1/2)_g$, are almost independent of each other and their abundances are expected to be mainly determined by the mechanisms leading to their creation rather than subsequent collision dynamics. However, further calculations are needed, both those focusing on the processes in which the $Kr_2^+$ molecular ions are formed as well as those responsible of the relaxation of nascent electronic excitations, to shed light on this still not fully resolved issue.

**Acknowledgments**

René Kalus and Cyril Van de Steen express their thanks to the Ministry of Education, Youth and Sports of the Czech Republic for the financial support from the *National Programme of Sustainability* (NPS II) project (grant no. LQ1602) and the *Large Infrastructures for Research, Experimental Development and Innovations* project (grant

no. LM2015070), as well as to VSB-TUO (grant no. SP2018/178). Traveling support from the Barrande programme of French-Czech collaboration (grants no. 40688TH and 8J18FR031) is also warmly acknowledged. The calculations have been performed using the resources of the IT4Innovations National Supercomputing Center of the Czech Republic (grant no. OPEN-13-2) and multiprocessing work stations of the parallel computational center of Toulouse.

[1] H. Helm and M. T. Elford, J. Phys. B **11**, 3939 (1978).

[2] H. Helm, Phys. Rev. A **14**, 680 (1976).

[3] M. Laroussi, IEEE Trans. Plasma Sci. **37**, 714 (2009).

[4] A. I. Bugrova, A. M. Bishaev, A. V. Desyatskov, M. V. Kozintseva, A. S. Lipatov, and M. Dudeck, Int. J. of Aero. Eng. **2013**, ID 686132 (2013).

[5] Q. Li, X.-M. Zhu, J.-T. Li, and Y.-K. Pu, J. Appl. Phys **107**, 043304 (2010).

[6] K. Hiraoka and T. Mori, J. Chem. Phys. **92**, 4408 (1990).

[7] Asterisk in Eq. 2 denotes an electronically excited Rg atom.

[8] H. Helm, J. Phys. B **9**, 2931 (1976).

[9] D. Hrivňák, R. Kalus, and F. X. Gadéa, Europhys. Lett. **71**, 42 (2005).

[10] H. Yoshii, T. Hayaishi, T. Onuma, T. Aoto, Y. Morioka, and K. Ito, J. Chem. Phys. **117**, 1517 (2002).

[11] H. Yoshii, K. Tsukamoto, T. Hayaishi, T. Aoto, K. Ito, and Y. Morioka, J. Chem. Phys. **123**, 184303 (2005).

[12] C. Van de Steen, M. Benhenni, R. Kalus, R. Ćosić, S. Illésová, F. X. Gadéa, and M. Yousfi, Plasma Sources Sci. Technol. **28**, 035007 (2019).

[13] Supplementary information material available at TO BE ADDED.

[14] C. Van de Steen, M. Benhenni, R. Kalus, B. Lepetit, F. X. Gadea, and M. Yousfi, Plasma Sources Sci. Technol. **27**, 065005 (2018).

[15] F. O. Ellison, J. Am. Chem. Soc. **85**, 3540 (1963).

[16] P. J. Kuntz and J. Valldorf, Z. Phys. D **8**, 195 (1988).

[17] M. Amarouche, G. Durand, and J. P. Malrieu, J. Chem. Phys. **88**, 1010 (1988).

[18] J. S. Cohen and B. I. Schneider, J. Chem. Phys. **61**, 3230 (1974).

[19] R. Kalus, I. Paidarová, D. Hrivňák, P. Paška, and F. X. Gadéa, J. Chem. Phys **294**, 141 (2003).

[20] T.-K. Ha, P. Rupper, A. Wuest, and F. Merkt, Mol. Phys. **101**, 827 (2003).

[21] J. Fedor, O. Echt, K. Głuch, S. Matt-Leubner, P. Scheier, and T. D. Märk, Chem. Phys. Letters **437**, 183 (2007).

[22] A. K. Dham, A. R. Allnatt, W. J. Meath, and R. A. Aziz, Mol. Phys. **67**, 1291 (1989).

[23] J. Sugar and A. Musgrove, J. Phys. Chem. Ref. Data **20**, 859 (1991).

[24] P. Ehrenfest, Z. Phys. **45**, 455 (1927).

[25] The mass of atomic nuclei, $m_\alpha$, has been set to an effective value obtained as a weighted average of atomic masses of all the stable isotopes of krypton ($\bar{M}_\mathrm{r} = 83.798$). As shown previously [14], such an approximation leads to a negligible error as compared with properly weighted cross-sections calculated for all the possible combinations of krypton isotopes in the collision complex.

[26] I. Janeček, D. Hrivňák, R. Kalus, and F. X. Gadéa, J. Chem. Phys. **125**, 104315 (2006).

[27] I. Janeček, S. Cintavá, D. Hrivňák, R. Kalus, M. Fárník, and F. X. Gadéa, J. Chem. Phys. **131**, 114306 (2009).

[28] A. Chicheportiche, B. Lepetit, M. Benhenni, F. X. Gadea, and M. Yousfi, J. Phys. B: At. Mol. Opt. Phys. **46**, 065201 (2013).

[29] A. Chicheportiche, Ph.D. thesis, Université Toulouse III Paul Sabatier (2014), in French.

[30] M. Child, *Molecular Collision Theory* (Mineola, NY: Dover, 1996).

[31] A. Chicheportiche, M. Stachoň, M. Benhenni, F. X. Gadéa, R. Kalus, and M. Yousfi, J. Chem. Phys. **141**, 134302 (2014).

[32] M. Yousfi, A. Hennad, and O. Eichwald, J. of Appl. Phys. **84**, 107 (1998).

[33] In the inverse-method approach, a spherical core-potential is used to calculate the collision cross-sections within the semi-classical (JWKB) approximation to be further used in Monte Carlo computations of transport properties (e.g., the ion mobility). The adjustable parameters of the core-potetial are adjusted iteratively unless a satisfactory agreement is achieved with reference experimental data (the $Kr_2^+$ mobility in this work). See Ref. 12 for more details. Note also that even though the inverse-method approach contains significant approximations and is preferably intended for atom-atom collisions, it has been used with success in a series of preceding studies involving molecular ions [31, 36–38]. .

[34] D. Bonhommeau, T. Bouissou, N. Halberstadt, and A. Viel, J. Chem. Phys **124**, 164308 (2006).

[35] As discussed in Ref. [31], an observation that the mobility data calculated from the $\sigma_{\mathrm{NRS}}^{(\mathrm{MT1})}$ cross-sections lie above the $\sigma_{\mathrm{NRS}}^{(\mathrm{MT2})}$ mobility values (i.e., effectively, $\sigma_{\mathrm{NRS}}^{(\mathrm{MT1})}<\sigma_{\mathrm{NRS}}^{(\mathrm{MT2})}$ ) may indicate that, on average, the colliding dimer is internally excited during the collision when scattered in the forward direction ($\theta \leq \pi/2$) and de-excited if scatterd backward ($\theta \geq \pi/2$). For the excitation channel, both rotational-vibrational and electronic excitations may in principle contribute in the present case. For the de-excitation pathway, mainly electronic quenching should be responsible since the dimers start from their rotationally-vibrationally ground state (and even classcial artifacts of the hybrid method leading to rotational-vibrational energies lying below the zero-point energy may not be sufficient to account for the observed shift in the mobility data). Nevertheless, no quantitative assessment can be done from the present data and a more detailed calculation going beyond the scope of the present work will be needed to analyze the role of electronic transitions in the $Kr_2^+/Kr$ collisions.

[36] A. Chicheportiche, M. Benhenni, M. Yousfi, B. Lepetit, R. Kalus, and F. X. Gadéa, Phys. Rev. E **88**, 043104 (2013).

[37] M. Benhenni, M. Stachoň, F. X. Gadéa, M. Yousfi, and R. Kalus, J. Phys. B: At. Mol. Opt. Phys. **49**, 175205 (2016).

[38] C. Van de Steen, M. Benhenni, R. Kalus, R. Ćosić, S. Illésová, F. X. Gadéa, and M. Yousfi, Phys. Chem. Chem. Phys. **21**, 7029 (2019).

## Figures and Tables

TABLE I: Equilibrium distances ($r_e$), classical binding energies ($D_e$), and binding energies with the zero-point correction included ($D_0$) calculated for various electronic states of the $Kr_2^+$ ion. The distances are given in Å and energies in eV. Corresponding values reported [22] for the neutral dimer, $Kr_2$, are as follows: $r_e = 4.011$Å and $D_e = 0.017$ eV.

| | model A [19] | | model B [20] | |
|---|---|---|---|---|
| state | $r_e$ | $D_e$ ($D_0$) | $r_e$ | $D_e$ ($D_0$) |
| $I(1/2)_u$ | 2.69 | 1.147 (1.136) | 2.70 | 1.177 (1.165) |
| $I(3/2)_g$ | 3.31 | 0.198 (0.193) | 3.32 | 0.186 (0.181) |
| $I(3/2)_u$ | 4.09 | 0.049 (0.047) | 4.21 | 0.032 (0.030) |
| $I(1/2)_g$ | 5.59 | 0.013 (0.012) | 6.11 | 0.006 (0.006) |
| $II(1/2)_u$ | 3.73 | 0.136 (0.132) | 3.72 | 0.120 (0.117) |
| $II(1/2)_g$ | 4.63 | 0.026 (0.025) | 4.82 | 0.013 (0.013) |

FIG. 1: Potential energy curves corresponding to six lowest electronic states of the $Kr_2^+$ ion. For comparison, the ground-state potential of the neutral dimer (shifted upward along the vertical axis by the value of Kr ionization potential calculated with the spin-orbit interaction in $Kr^+$ neglected) is also shown as a thick grey curve plotted in the background.

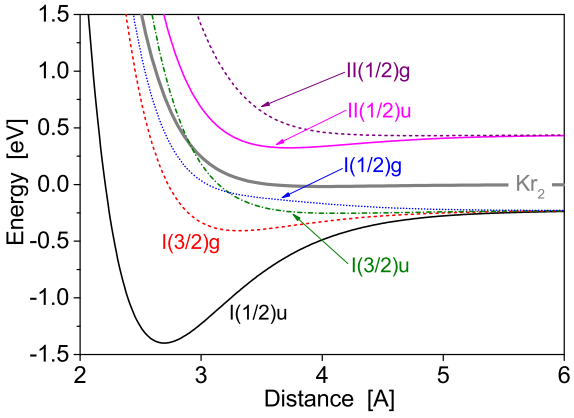

FIG. 2: Reduced mobility of the $Kr_2^+$ ion initially in one of the group I electronic states: circles – $I(1/2)_u$, diamonds – $I(3/2)_g$, hexagons – $I(3/2)_u$, and squares - $I(1/2)_g$, and in corresponding rotational-vibrational ground states, $[j = 0, v = 0]$. Mobility calculations have been performed using the $\sigma_{NRS}^{(MT2)}$ cross-sections (Eq. (9)), full symbols correspond to cross-sections obtained for model A, empty symbols represent data calculated for model B. Dash-dotted (model A) and dashed (model B) curves close to respective symbols correspond to mobilities calculated using the $\sigma_{NRS}^{(MT1)}$ cross-sections (Eq. (8)). For comparison, experimental data reported for the $Kr_2^+/Kr$ mobility [1] are also shown (grey balls) together with their inverse-method extrapolation [12] (grey dots). In the inset, averaged $I(1/2)_u$ and $I(3/2)_g$ mobilities (crosses) are shown for comparison as calculated for model B and kind 2 MT cross-sections. Respective weights have been set to $w = 0.7$ and $w = 0.3$.

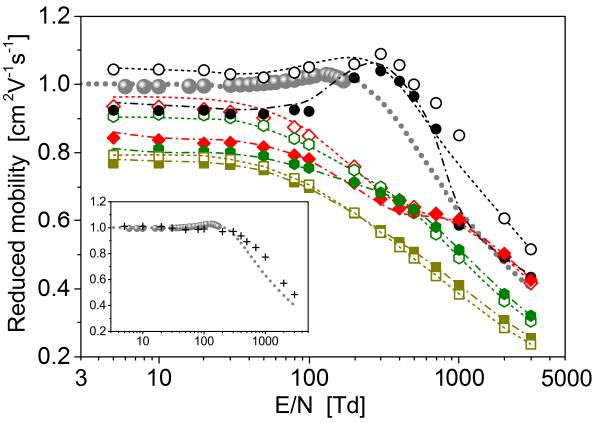

FIG. 3: Reduced mobility of the $Kr_2^+$ ion initially in one of the group II electronic states: up triangles – $II(1/2)_u$, and down triangles – $II(1/2)_g$, and in corresponding rotational-vibrational ground states, $[j = 0, v = 0]$. Other symbols and line patterns are the same as in Fig. 2. In addition, full (model A) and empty (model B) circles are added for illustration and correspond to $II(1/2)_u$ and $II(1/2)_g$ mobilities calculated from kind 2 MT cross-sections (Eq. (9)) and averaged with equal weights.

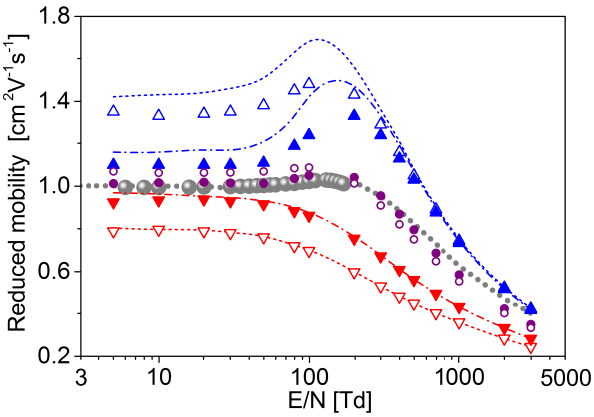

FIG. 4: Dependence of the mobility of $Kr_2^+$ ion, initially in the $II(1/2)_u$ electronic state, on its initial vibrational (full symbols) and rotational (empty symbols) state as calculated for model A and the kind 2 MT cross-sections (Eq. (9)): bullets – rotational-vibrational ground state, $[j = 0, v = 0]$, up triangles $[j = 0, v = 2]$ ($\Delta E \approx 13\,\mathrm{meV}$), down triangles $[j = 0, v = 5]$ ($\Delta E \approx 31\,\mathrm{meV}$), and diamonds $[j = 0, v = 10]$ ($\Delta E \approx 58\,\mathrm{meV}$); empty down triangles $[j = 100, v = 0]$ ($\Delta E \approx 35\,\mathrm{meV}$) and empty diamonds $[j = 130, v = 0]$ ($\Delta E \approx 59\,\mathrm{meV}$). For comparison, experimental data [1] (grey balls) and corresponding inverse-method data [12] (gray dots) are also included. Note also that lines, contrary to Figs. 2 and 3, do not represent kind 1 MT data and are just added to guide eyes.

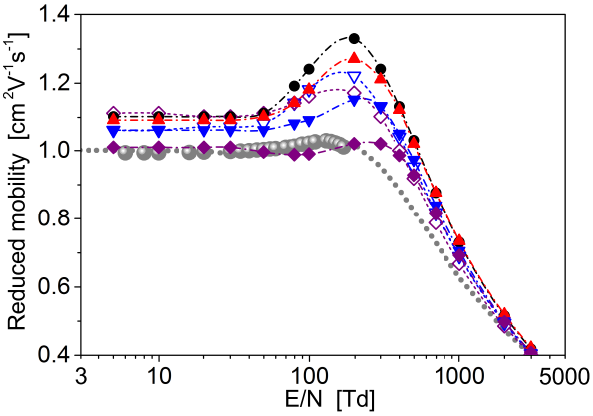

FIG. 5: Dimer ion disappearance (DID) rate constants of the $Kr_2^+$ ion initially occupying one of the electronic states of group I (circles – $I(1/2)_u$, diamonds – $I(3/2)_g$, hexagons – $I(3/2)_u$, and squares - $I(1/2)_g$) and/or group II (up triangles – $II(1/2)_u$, and down triangles – $II(1/2)_g$) as calculated from DID cross-sections (Eq. (10)) and kind 2 MT cross-sections (Eq. (9)) for $[j = 0, v = 0]$. Full symbols correspond to data obtained for model A, empty symbols represent data calculated for model B. In the inset, DID cross-sections calculated using interaction model A are displayed against the $Kr_2^+$/Kr center-of-mass collision energy. Like in Fig. 4 and contrary to Figs. 2 and 3, lines do not represent kind 1 MT cross-sections data and are just added to guide eyes.

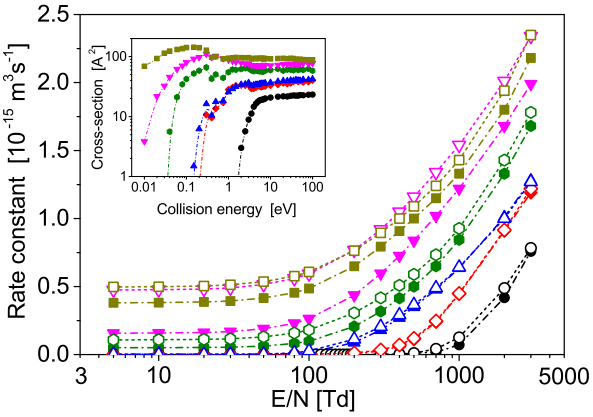

FIG. 6: Dimer ion disappearance (DID) rate constants of the $Kr_2^+$ ion initially occupying the $II(1/2)_u$ electronic state and various rotational-vibrational states as calculated for model A and using kind 2 MT cross-sections (Eq. (9)): full bullets $[j = 0, v = 0]$, full up triangles $[j = 0, v = 2]$, full down triangles $[j = 0, v = 5]$, full diamonds $[j = 0, v = 10]$, empty down triangles $[j = 100, v = 0]$, and empty diamonds $[j = 130, v = 0]$. Notice a break and the change of a log scale to a linear scale on the vertical axis at the value of 0.05. In the inset, corresponding DID cross-sections are depicted for completeness.

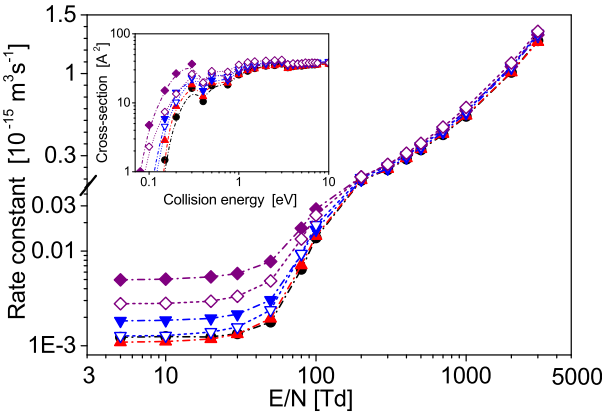

FIG. 7: Total cross-sections (full bullets) of the dimer ion disappearance (DID) channel obtained for the dimer ion initially occupying the $\mathrm{II}(1/2)_g$, $[j = 0, v = 0]$ state and decomposed to the charge transfer (CT, empty circles) and collision induced dissociation (CID, empty diamonds) components. In the inset, probabilities of the CT channel are plotted, for selected collision energies (indicated as short arrows in the main panel), against the impact-parameter: solid line $E_{\mathrm{coll}} = 0.08\,\mathrm{eV}$, dashed line $E_{\mathrm{coll}} = 0.3\,\mathrm{eV}$, dash-dotted line $E_{\mathrm{coll}} = 0.4\,\mathrm{eV}$, dash-dot-dotted line $E_{\mathrm{coll}} = 2\,\mathrm{eV}$, and dotted line $E_{\mathrm{coll}} = 20\,\mathrm{eV}$. All the calculations have been performed using interaction model A.